Computed SAR and Thermal Elevation in a 0.25mm 2D Model of the Human Eye and Head in response to an Implanted Retinal Stimulator. Part II: Results

Gianluca Lazzi, *Senior Member, IEEE*, Stephen C. DeMarco, Wentai Liu, *Senior Member, IEEE*, James D. Weiland, *Member, IEEE*, and Mark S. Humayun, *Member, IEEE*

***Abstract*—This is the second of a series of two papers on the thermal increase in the human eye and head in response to an implanted retinal stimulator. This paper provides Specific Absorption Rates (SARs) induced in the human head by the extra-ocular unit and the temperature increases associated with induced electromagnetic fields and power dissipation of the implanted microchip. Results are provided for different assumptions about choroid blood flow as well as for different thermal conductivities of the implanted microchip to account for differences in thermal behavior arising from variations in the material composition of the implant and its hermetically-sealed biocompatible case. It is shown under the expected worst case operating conditions that computed results associated with the power dissipation of the implanted microchip under the assumption of silicon composition for the entire chip, corresponding to temperature increases of approximately 0.6°C in the eye and 0.2°C in the retina, closely parallel *in-vivo* experimental results in animals.**

***Index Terms*—Retinitis-Pigmentosa, Age-Related Macular Degeneration, Retina-Prosthesis, FDTD, SAR, Temperature, Thermal-Simulation, Stimulator-IC**

I. Introduction

The specific absorption rate and the dissipated stimulator IC power are the mechanisms which are expected to account for the ocular heating. Therefore, the numerical FDTD method for specific absorption rate (SAR) computation and the numerical thermal method in Part I are applied to the newly developed truncated head/eye model to estimate the increase in temperature. In order to gain further insight into the results, the influence of SAR and dissipated power in the implant are considered separately.

II. Specific Absorption Rate (SAR)

In a typical application of NCSU's *Retina-3.5* microstimulator [1] in which it is assumed that the implant is operating with all channels active at current levels 100% of maximum specifications, required continuous supply currents of 10mA were predicted. Experiments with inductive coupling based on the work in [2], showed that a power of 200Vpp at 2A in the primary coil was necessary to obtain 10mA of source current at V_{dd}=5v and V_{ss}=−5v on the secondary side (power receiving coil). Therefore, the Specific Absorption Rate (SAR) distribution resulting from the numerical FDTD at 2MHz has been linearly scaled to reflect the primary side input power used in these experiments. A color-mapped graphical representation of the resulting SAR is provided in Figure 1. The transmitter coil was constructed with a 2-inch diameter and 10 turns. In two-dimensional simulation, it is represented as two point sources of opposite polarity and is positioned as indicated in Figure 1 above the left eye at a location consistent with attachment to a pair of framed reading glasses. The truncated head/eye model is surrounded with 50 PML layers and then excited with the $\vec{\mathbf{H}}$-field sourced from the 2D coil.

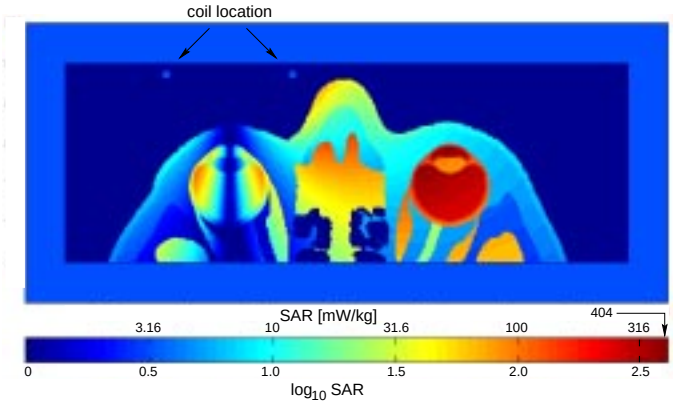

Fig. 1. Specific absorption rate in log scale at 2MHz irradiation for 2A coil current

Results in Figure 1 show the power levels which are scaled to $\frac{\text{mW}}{\text{kg}}$ and are provided in $\log_{10}$ scale for best viewing with the linear scale added for reference. The SAR distribution shows that the right eye receives more deposited power than the targeted left eye containing the prosthesis. The major reason for the location of this peak SAR in the right eye is the much higher conductivity of the eye humor with respect to other organs, such as cartilage, bone, or skin. The eye with the prosthesis is exposed to minimal electric field (electric field on the axis of the coil is ideally zero) while the largest electric field is found on the sides of the coil. Thus, the opposite eye is exposed to large electric fields compared to organs normal to the axis of the coil and, considering the higher conductivity of the eye humor, this results in relatively high SAR compared to other organs.

G. Lazzi, S.C. DeMarco, and W. Liu are with the Dept. of Electrical and Computer Engineering, NC State University, Raleigh, North Carolina, USA. The Work of G. Lazzi is supported in part by the Whitaker Foundation under contract RG-00-0298 and in part by NSF CAREER award number 0091599. The work of W. Liu is supported in part by NSF award number BES-9808040 and in part by NIH.

J. D. Weiland and M.S. Humayun are with the Doheny Eye Institute at the University of Southern California, Los Angeles, California, USA. The work J.D. Weiland and M.S. Humayun is supported in part by NSF award BES-9810914 and in part by NIH.

III. The Influence of Choroidal Blood Flow on Ocular Temperature

Studies have revealed a relation between damage to the photoreceptor layer of the retina and ocular temperature [3], [4]. Anterior to the human retina's photoreceptor layer and to the pigmented epithelium lies the choroid which is a vascularized layer supplying blood to the outer retina. The blood circulation density to the outer retina by way of the choroid is known to be higher than in any other bodily tissue [5], [6]. In fact, the blood flow exceeds the oxygenation needs of the outer retina and the retinal pigment epithelium [5], [6]. It is proposed that the high blood flow from the choroidal layer facilitates the regulation of retinal temperature which would otherwise increase in the outer retina during the photo-transduction of incident light and absorption in the epithelium of excess light energy [7]. Experiments revealed that less energy from incident light was necessary in dead animals than in living animals to incur retinal damage [5]. Furthermore, reducing blood flow in living animals also encouraged retinal damage from light energy. Other studies revealed a type of closed loop neural feedback in which increased energy from incident light produced an increase in choroidal blood flow [8], [9].

In order to gain insight into the influence of choroidal blood flow on ocular cooling, numerical simulations are conducted to compare thermal results first assuming no choroidal blood flow in the head/eye model of Figure 8 from Part I and subsequently with blood flow modeled. Under both assumptions, the choroid is not considered blood, but is instead identified as an independent, unique tissue type. However, because it is heavily vascularized, it is modeled with the same dielectric and thermal properties and mass density of blood.

IV. Thermal Simulations in the Absence of Choroidal Blood Flow

We first consider the absence of choroidal blood flow wherein the temperature of the choroidal tissue is allowed to rise as dictated by the bioheat equation, as any other tissue type would when exposed to heat. Note that the retina is assigned a high blood perfusion constant in Table IV from Part I, wherein the source of this blood is the adjacent choroidal tissue. Thus, we impose the additional constraint that the parameter of T_b occurring in the bioheat equation when evaluating retinal temperature will be replaced with the computed temperature of the choroid, and will not be considered fixed at 37°C as is the case for other tissues, which are perfused with flowing blood. Thus, we consider a fixed blood temperature, T_b=37°C, for all perfused tissues except retina and a variable blood temperature, $T_{choroid} \neq T_b$, in lieu of the retina. The cooling term in the bioheat equation will be $-B(T - T_b)$ for non-retinal tissue and $-B(T - T_{choroid})$ for retina.

A. Initial temperature distribution

As we are interested in the temperature increase above the natural temperature distribution, it is necessary to first simulate thermal spread in the head/eye model of Figure 7 from Part I, beginning at an initial assumed air temperature of 24°C, while devoid of the influence of SAR and of the implanted IC. The results of this simulation appear consistent with expectations of the natural temperature distribution in the human head. A peak temperature of 37.2857°C occurs within the brain due to the high basal metabolism associated with white and grey matter as seen in Table IV from Part I. Cooler temperatures occur near the interface between the head model and the surrounding air where thermal convection occurs.

The anterior portion of the initial temperature distribution corresponding to the truncated head/eye model of Figure 8 from Part I is then isolated (Figure 2) to provide a starting point for predicting thermal increase above the natural temperature distribution due to SAR and the implanted microchip. In this front portion of the head model, a peak temperature of 37.1094°C occurs in the brain.

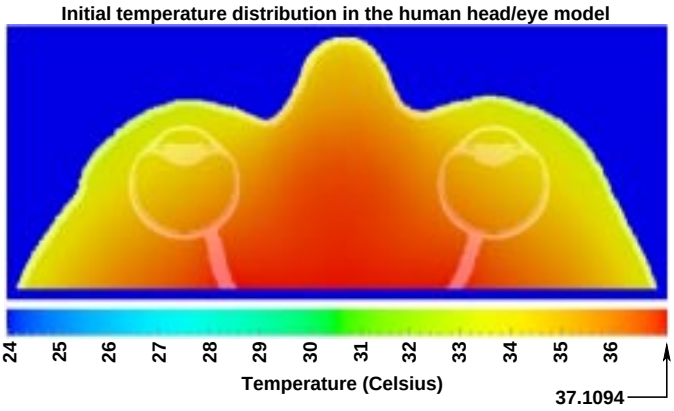

Fig. 2. Initial temperature distribution (anterior portion) in the human head/eye model in the absence of choroidal blood flow and with no excitation from SAR or from the stimulator IC

B. Temperature increase due to SAR

A thermal simulation predicting the temperature increase arising from the SAR of Figure 1 applied to the head/eye model of Figure 8 from Part I is run with a simulated time coverage of one hour. At the end of one hour of simulated time, the peak temperature rise in the right eye has converged to a value of 0.0685°C and the rate of increase has diminished to approximately 10^{-7} °C when monitored at 0.5s intervals.

A plot of temperature increase over time due to SAR for the left and right eyes is provided in Figure 3a. The vertical axis represents the maximum increase above the initial temperature distribution encountered over each eye. The SAR distribution of Figure 1 indicates most of the power is deposited in the right eye despite targeting the stimulator IC in the left eye, owing to the $\vec{\mathbf{E}}$–field distribution associated with the $\vec{\mathbf{H}}$–field sourced from the primary coil. Accordingly, the peak thermal increase of 0.0685°C also occurs in the right eye. Note that the temperature rise in each eye asymptotically approaches steady state as heat continues to spread beyond the eyes and into the surrounding head tissues.

A color-mapped graphical plot of the steady state temperature distribution resulting from the SAR of Figure 1 is provided in Figure 3b. The maximum temperature increase of 0.0685°C is indicated by the red area near the lens of the right eye. Once again, this is consistent with the location of the SAR maximum

from Figure 1.

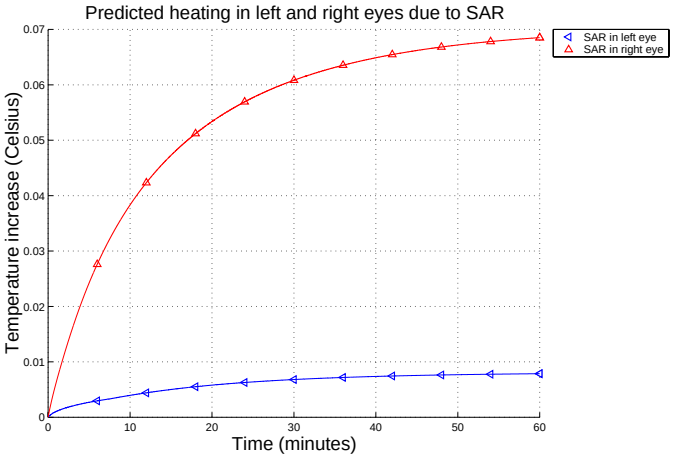

(a) Temperature increase versus time

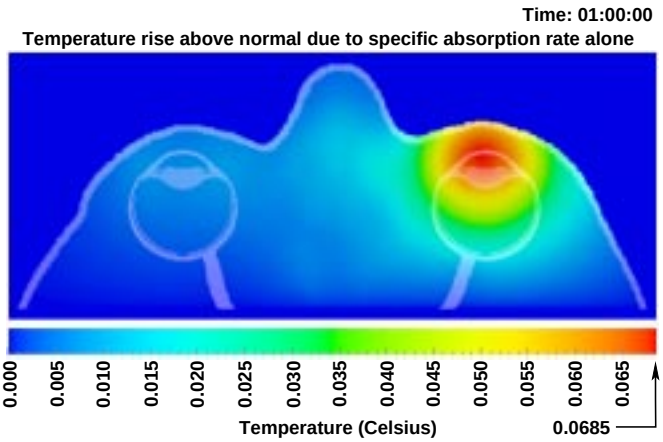

(b) Steady state distribution after 60 minutes

Fig. 3. Predicted ocular heating in the head/eye model due to SAR in the absence of choroidal blood flow

C. *Temperature increase due to power dissipation in the implanted stimulator IC*

The stimulator power estimates of Table II from Part I acquired from *Hspice* simulation have been passed to the thermal numerical method developed in Section II from Part I in order to predict ocular heating. These values correspond to $P_{chip(3D)}$ and are used to compute $P^{(density)}_{\underline{chip(2D)}\ \underline{(discrete)}}(i,j)$ in Equation 3 from Part I, according to derivation in section IV from Part I. A separate thermal simulation has been conducted for each of the twelve variations in biphasic stimulus currents. As with the simulations of thermal increase due to SAR, the initial temperature distribution of Figure 2 is assumed at the start of each simulation.

A plot of temperature increase in the left eye over time for the twelve stimulation cases is provided in Figure 4a. Again, the vertical axis represents the maximum increase above the initial temperature distribution for the left eye of Figure 8 from Part I in which the stimulator IC is modeled. Notice again the asymptotic convergence of temperature rise in the left eye occurring for each power scenario, as heat spreads beyond the confines of the left eye.

A color-mapped graphical plot of the predicted steady state temperature distribution arising from operation of the stimulator IC is provided in Figure 4b, corresponding to the expected worst case power dissipation, $P_{chip(3D)} = 46.4672$mW from Table II from Part I. A maximum temperature increase of 0.6123°C is indicated over the region of the IC in the left eye. At the surface of the retina, the temperature increase appears to be near 0.2°C–0.25°C.

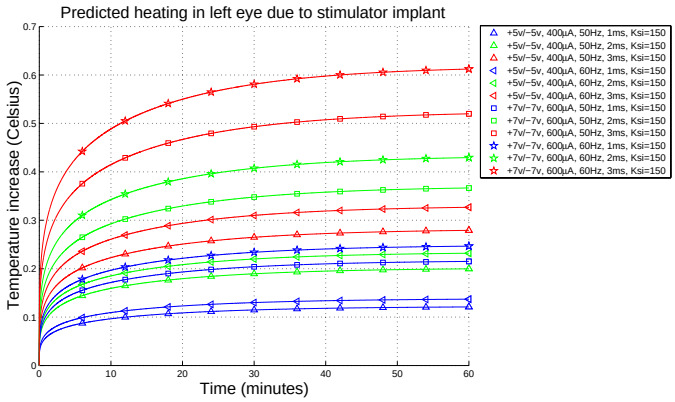

(a) Temperature increase versus time

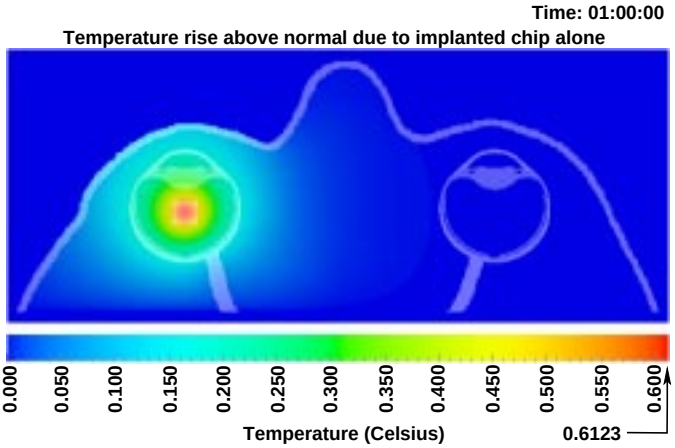

(b) Steady state distribution after 60 minutes

Fig. 4. Predicted ocular heating in the head/eye model due to stimulator implant power in the absence of choroidal blood flow

V. Thermal Simulations in the Presence of Choroidal Blood Flow

Since, the blood flow rate is considered to vary with incident light energy [8], [9], the heat dissipating influence of flowing blood is modeled by holding the choroidal temperature at $T_b = 37$°C, thereby assuming ideally an "infinite" blood flow. In the biological system, the blood is expected to increase above

$T_b = 37°C$ as it carries away heat absorbed in the outer retina and pigmented epithelium. But as it quickly circulates and is replaced by fresh blood, we assume that a fixed choroidal temperature of $T_{choroid} = T_b = 37°C$ in the head/eye model of Figure 8 from Part I closely approximates the true response of the choroid.

A. Initial temperature distribution

In section IV-A the initial steady state temperature distribution in the absence of choroidal blood flow was computed as a starting point for simulations predicting thermal increase. Similarly, a new initial distribution is computed in the presence of choroidal blood flow. Once again, this is obtained by assuming a fixed choroidal blood temperature of $T_b = 37°C$ and is computed beginning with an air temperature of 24°C and devoid of the influence of SAR and the implant IC.

The anterior portion of the initial temperature distribution corresponding to the truncated head/eye model of Figure 8 from Part I is again isolated from the initial distribution as shown in Figure 5. This new initial temperature distribution clearly highlights the choroidal blood flow now accounted for in thermal simulation, as can be seen in the region posterior to the retina in both eyes as compared with the same areas in Figure 2 where choroidal blood flow was not included. Thus, this new truncated initial distribution will serve to initialize the thermal simulations of SAR and of the implant IC in the context of blood flow in the choroid. A peak temperature of 37.2159°C occurs in the anterior portion of the initial temperature distribution, resulting from a forced choroidal blood temperature of $T_b = 37°C$. This forced blood temperature in conjunction with heating from the brain with its high basal metabolism results in a peak temperature within the region slightly in excess of the 37.1094°C encountered in Figure 2.

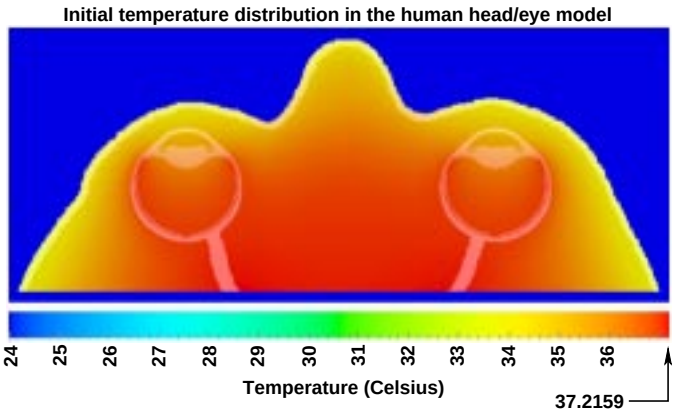

Fig. 5. Initial temperature distribution (anterior portion) in the human head/eye model in the presence of choroidal blood flow and with no excitation from SAR or from the stimulator IC

B. Temperature increase due to SAR

Under the assumption of fixed choroidal temperature, a thermal simulation predicting the temperature increase arising from the SAR of Figure 1 is again run with a simulated time coverage of one hour. After one hour of simulated time, the peak temperature rise in the right eye has converged to a value of 0.0479°C.

A plot of temperature increase over time due to SAR for the left and right eyes is provided in Figure 6a. In contrast to the curves of Figure 3, the temperature increases for both eyes appear to reach steady state around 35-40 minutes. The reason for this rapid convergence is that the fixed blood of 37°C in the eyes prevents heat from spreading across the choroid as can be clearly seen in the color-mapped graphical plot of the steady state temperature distribution resulting from the SAR of Figure 1 as provided in Figure 6b. This is strong contrast to the situation present in Figure 3 where the diffusion of heat does occur across the choroid where its temperature is not forced at 37°C. The maximum temperature increase of 0.0479°C is indicated by the red area concentrated in the aqueous humor of the anterior chamber forward of the lens. The fact that the isotherms over the right eye of Figure 6b do not cross over the choroid as they do in Figure 3b. This further indicates that the choroid is acting to provide thermal regulation. This is no longer evident near the vitreous base and over the cornea where the SAR-induced heat expands beyond the boundaries of the right eye.

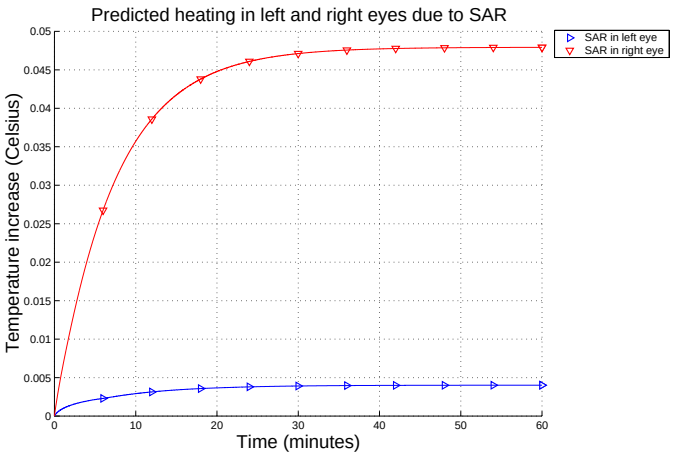

(a) Temperature increase versus time

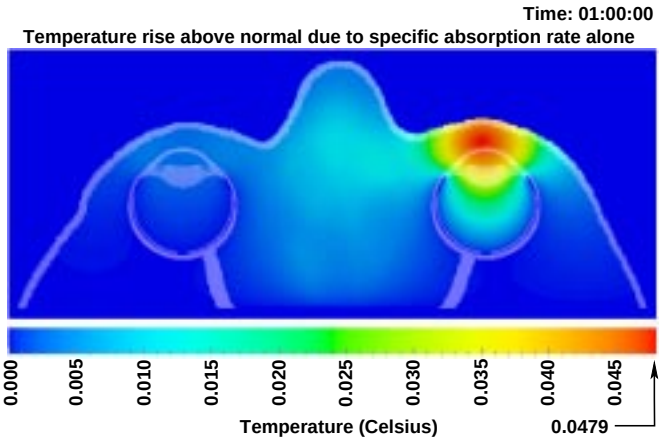

(b) Steady state distribution after 60 minutes

Fig. 6. Predicted ocular heating in the head/eye model due to SAR in the presence of choroidal blood flow

TABLE I

TEMPERATURE ELEVATIONS RESULTING FROM THE THERMAL SIMULATION OF SAR, CORRESPONDING TO FIGURE 1, IN THE ABSENCE OF CHOROIDAL BLOOD FLOW

Model region[1]	Maximum SAR $\left[\frac{\text{mW}}{\text{kg}}\right]$	Peak increase above the initial temperature $\Delta T = T - T_0$ [°C]	
		(− blood)[2]	(+ blood)[3]
over left eye	111.9966	0.0079	0.0040
over right eye	404.1180	0.0685	0.0479

[1]Corresponds to the head/eye model of Figure 8 from Part I.

[2]These results represent the maximum temperature increase in the left and right eyes between the initial and final temperature distributions in the absence of choroidal blood flow.

[3]Similarly, these results also represent maximum temperature increase, but now in the presence of choroidal blood flow.

C. *Temperature increase due to power dissipation in the implanted stimulator IC*

Again under the assumption of fixed choroidal temperature, thermal simulations are once more run for each of the twelve stimulation cases, using microchip power estimates from Table II from Part I, in order to predict ocular heating in the left eye due to the stimulator implant.

A plot of temperature increase in the left eye over time for the twelve stimulation cases is provided in Figure 7a. As with the SAR-induced heating in the context of choroidal blood flow, the temperature increases again appear to converge to steady state within 30 minutes.

A color-mapped graphical plot of the predicted steady state temperature distribution arising from operation of the stimulator IC is provided in Figure 7b, corresponding to the expected worst case power dissipation, $P_{chip(3D)} = 46.4672$mW from Table II from Part I. Due to the fixed temperature of the choroid, a reduced maximum temperature increase of 0.4349°C is now indicated over the region of the IC in the left eye. The temperature increase appears minimal near the surface of the retina. In contrast to Figure 4b, where heat from the stimulator IC expands beyond the eye region and into the surrounding head tissues, Figure 7b indicates a larger portion of the heat is localized by the choroid. Only near the anterior of the eye where the choroid ends do we see heat spreading beyond the left eye boundary.

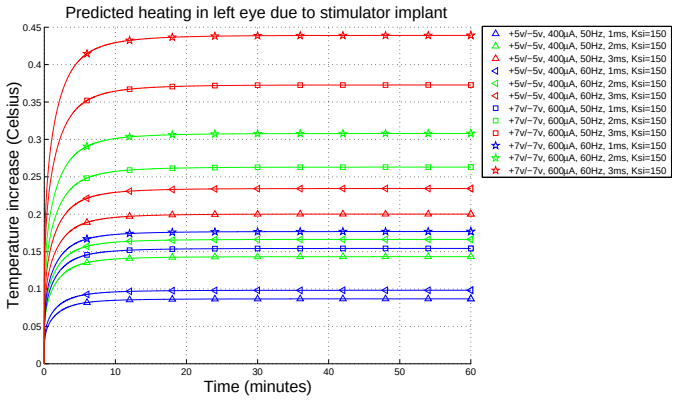

(a) Temperature increase versus time

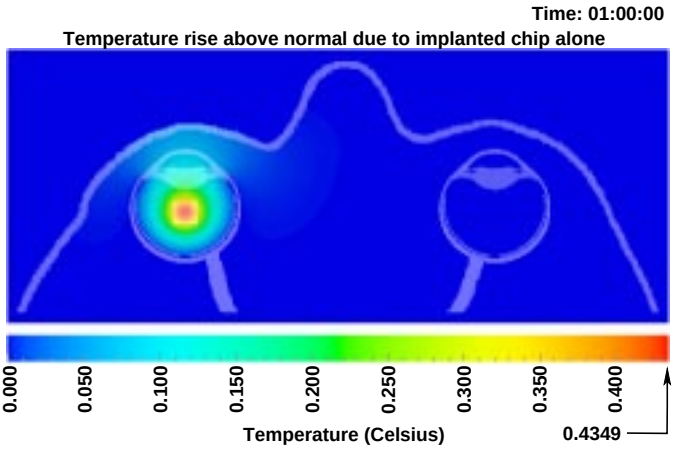

(b) Steady state distribution after 60 minutes

Fig. 7. Predicted ocular heating in the head/eye model due to stimulator implant power in the presence of choroidal blood flow

VI. COMPARISON OF THERMAL RESULTS WITH AND WITHOUT CHOROIDAL BLOOD FLOW

The numerical simulations of sections IV and V clearly indicate the potential benefit which may be afforded to an implantable prosthesis by the blood flow of the choroid. In regards to SAR, notice that the amount of cooling is more prominent in the right eye where the SAR (deposited electromagnetic power) is greater. The maximum temperature in the right eye is lower by 0.0206°C for a decrease of 30.07% while the maximum in the left eye is lower by 0.0039°C for a decrease of 49.37%, as summarized in Table I.

Similar comparisons are provided for ocular heating due to power dissipation in the stimulator IC, which take into account the twelve simulated variations in biphasic stimulus currents. In the worst operating conditions considered, corresponding to biphasic stimulus currents of 600μA amplitude at 60Hz repetition rate and 3ms pulse width, the maximum temperature increase over the left eye while accounting for blood flow in the choroid is lower by 0.1774°C for a decrease of 28.97% with respect to maximum temperature rise obtained with no blood flow. This comparison for the worst case and the remaining operating conditions considered is summarized in Table II.

A further comparison of the thermal simulation results with and without choroidal blood flow is provided in Figure 8. Temperature increase in the left eye for the twelve operating scenarios is plotted versus stimulator IC power. The upper bounding curve represents a least squares linear fit to the thermal results in the absence of choroidal blood flow, while the lower bounding curve represents a fit to the thermal results in the presence of choroidal blood flow.

The grey-shaded region between the bounding curves represents the uncertainty region, wherein the actual temperature in-

TABLE II

TEMPERATURE ELEVATIONS RESULTING FROM THE *Hspice* SIMULATED POWER DISSIPATION ESTIMATES, $P_{chip(3D)}$, OF TABLE II FROM PART I, IN THE ABSENCE OF CHOROIDAL BLOOD FLOW

V_{dd}, V_{ss} $[V_{DC}]$	current A $[\mu A]$	frame rate $f=\frac{1}{T}$ [Hz]	pulse width W [ms]	Simulated chip power[1] $P_{chip(3D)}$ [mW]	Peak increase above the initial temperature[2] $\Delta T = T - T_0$ [°C] (−blood)[3]	(+blood)[4]
$^{+}5,^{-}5$	400	50	1	9.1862	0.1210	0.0860
$^{+}5,^{-}5$	400	50	2	15.1580	0.1997	0.1419
$^{+}5,^{-}5$	400	50	3	21.1874	0.2792	0.1983
$^{+}5,^{-}5$	400	60	1	10.4012	0.1371	0.0974
$^{+}5,^{-}5$	400	60	2	17.6018	0.2319	0.1648
$^{+}5,^{-}5$	400	60	3	24.8018	0.3268	0.2321
$^{+}7,^{-}7$	600	50	1	16.3216	0.2151	0.1528
$^{+}7,^{-}7$	600	50	2	27.8308	0.3667	0.2605
$^{+}7,^{-}7$	600	50	3	39.4527	0.5198	0.3693
$^{+}7,^{-}7$	600	60	1	18.7112	0.2465	0.1751
$^{+}7,^{-}7$	600	60	2	32.5892	0.4294	0.3050
$^{+}7,^{-}7$	600	60	3	46.4672	0.6123	0.4349

[1]Duplicated from Table II from Part I.

[2]Absolute temperatures are omitted for brevity, as thermal increase above the initial distribution is the parameter of interest.

[3]These results indicate the maximum temperature increase over the left eye between the initial and final temperature distributions in the absence of choroidal blood flow.

[4]Similarly, these results also represent maximum temperature increase, but now in the presence of choroidal blood flow.

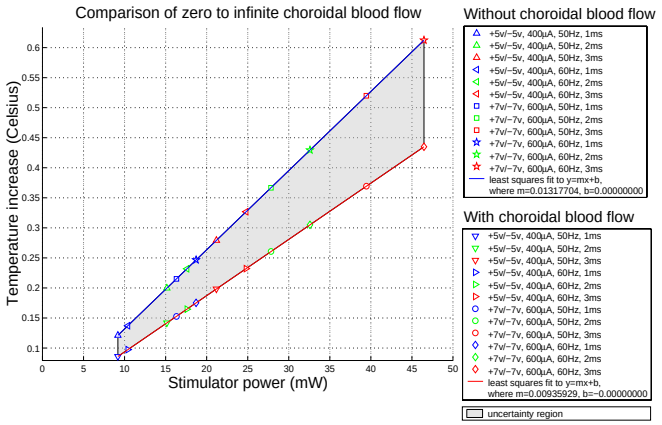

Fig. 8. A comparison of predicted ocular heating versus stimulator implant power while considering the absence and presence of choroidal blood flow

crease associated with the finite yet unknown blood flow rate is expected to occur. Since the infinite blood flow approximation considered in the simulations of section V is expected to closely model the response of the true biological system, realistic temperature elevations due to these power estimates are expected to track the lower curve much more closely that the upper curve. Maximum steady state temperature increase in the left eye tracks linearly with stimulator power dissipation both in the presence and absence of blood flow. Notice that as the power dissipation increases the difference between maximum temperature predictions for the presence and absence of blood flow also increases for corresponding stimulator IC operating conditions.

VII. EFFECT OF THE THERMAL CONDUCTIVITY OF THE STIMULATOR IC

All the results reported above are relative to a thermal conductivity of bare silicon. To gain insight into the effect that lower thermal conductivity will have on the temperature increase in the eye, due to variations in precise material composition of the stimulator IC, additional supporting intra-ocular components, and the hermetically-sealed biocompatible casing, we have repeated the study for thermal conductivities of the microchip ranging from $K_{chip} = 30$ to $K_{chip} = 150$. Each of these simulations has been repeated for the worst case scenario of dissipated power, corresponding to 46.4672 mW. Results are shown in Figure 9 for both cases of absence of choroidal blood flow and "infinite" choroidal blood flow. As expected, the case of an implanted system with a thermal conductivity lower than that of bare silicon shows higher temperature increase induced in the human eye, with an exponential-like decay as a function of the thermal conductivity. We are still in the process of determining the best biocompatible materials before we can make a clear assessment of the final thermal conductivity for the implanted portion of the prosthesis. Nonetheless, with the thermal conductivity of 150 for silicon, we expect the implanted system with all encapsulant materials accounted for to have a net effective thermal conductivity in excess of 100.

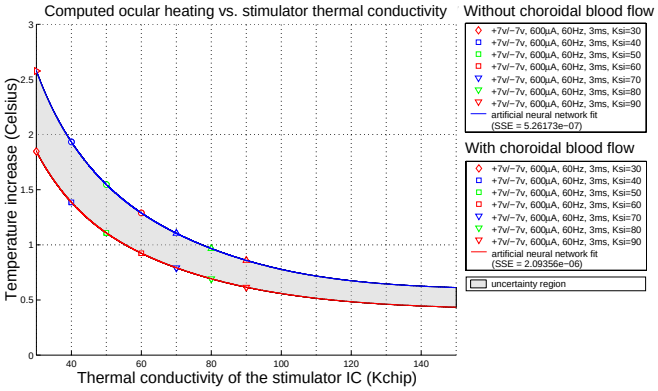

Fig. 9. A comparison of computed ocular heating versus thermal conductivity, K_{chip}, of the stimulator IC for expected worst case power dissipation, $P_{chip(3D)} = 46.4672$mW, while considering the absence and presence of choroidal blood flow. This heating is recorded at the location of the stimulator IC.

VIII. EXPERIMENTAL VALIDATION

In supplement of the analytical validations of the numerical methods presented in Section II from Part I [10], a further step has been taken to gain additional confidence in the thermal simulation results presented in Section IV and Section V. Researchers at the University of Southern California (formerly at Johns Hopkins University) have experimentally measured the thermal response to power dissipation introduced into the eyes of dogs [11]. In one of several experiments in this work, 500mW of power dissipation introduced intra-ocularly for a duration of two hours at midvitreous via a ceramic-tipped resistive heating element led to a 2°C increase in the temperature measured at the retina surface. The simulated thermal elevations encountered in the left eye versus the twelve power dissipations

considered for the stimulator IC as shown in Figure 8, represent the maximum elevation which occurred at the location of the stimulator IC model in Figure 8 from Part I. In order to correlate this data with this experimental measurement at USC/JHU [11], the simulated thermal elevation encountered at the retina surface is plotted versus the power dissipation in the stimulator IC as shown in Figure 10.

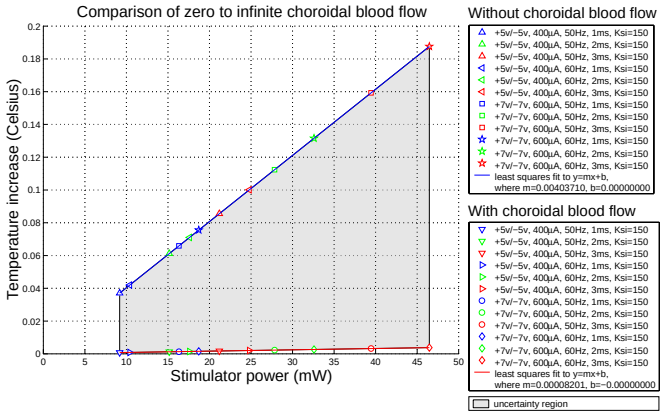

Fig. 10. A comparison of computed ocular heating over the left eye versus power dissipation in the stimulator IC while considering the absence and presence of choroidal blood flow. This heating occurs at the inner retinal surface near the fovea.

The upper line corresponds to the heating at the retinal surface in the absence of any choroidal blood flow. Conversely, the lower line is associated with retina heating where choroidal "infinite" blood flow is maintained. In the latter case, the fixed choroidal temperature of 37°C prevents the adjacent retina from heating as greatly as in the former case where the choroidal temperature is not held fixed. As such, a maximum simulated temperature elevation of only 0.0038°C is observed.

Based on the observed linear dependence of retinal heating over the range of power dissipations shown here, extrapolating the 500mW power dissipation used in the experiments at USC/JHU back down to $P_{chip(3D)} = 46.4672$mW (the highest power dissipation considered for the stimulator IC) would predict a thermal elevation of 0.1859°C. From the data associated with the case of no choroidal blood flow plotted in Figure 10, the thermal elevation encountered at the retinal surface for $P_{chip(3D)} = 46.4672$mW is 0.1876°C. This is in good agreement with the measured value from the Johns Hopkins experiment [11]. Although, the data from the John Hopkins experiment was measured on live eyes with choroidal blood flow, no significant changes were measured when choroidal blood flow was stopped partway through one of the experiments [11]. The lack of any observed variations in recorded temperatures during collection of experimental data indicates that the model with no blood flow is more close to reality than the model with infinite blood flow. This means that the blood vessels in the choroid are not such to maintain the choroidal temperature at a constant value of 37°C.

IX. Conclusion

We have presented a numerical study of the thermal increase in the human eye and head associated with the operation of an implantable retinal prosthesis to recover limited sight in blind patients affected by retinitis pigmentosa (RP) or age-related macular degeneration (AMD). The prosthesis system intends to provide electrical stimulation to existing living ganglion and bipolar cells of the retina using an array of on-chip stimulus circuits, and it uses inductive telemetry over coils for power and data communication. The demonstration that direct electrical stimulation of retinal ganglion cells can create visual sensation in patients has been shown clinically [12], [13], and patients have been able to recognize English characters and other simple forms when stimulated by a small array of retinal electrodes.

A new two-dimensional 0.25mm resolution cross-section of the human head has been developed with a novel semi-automatic discretizer to account for the finest anatomical details of the human eye. While a D-H FDTD method with PML absorbing boundary conditions has been used to compute the electromagnetic fields induced in the human head by the external telemetry coil, a discretized version of the bioheat equation accounting for both induced SAR and dissipated power of the implanted microchip has been developed to compute the temperature elevation in the human eye associated with the retinal prosthesis system.

We have concluded that in absence of choroidal blood flow, which corresponds to the case of blood flow rates that are not sufficient to carry away a significant amount of heat, a maximum temperature rise of 0.0685°C is induced by the external telemetry coil in the eye that does not contain the implanted microchip. Conversely, when considering choroidal blood flow, corresponding to the case of blood flow rates that are such to maintain the temperature of the choroid at a steady 37°C, a reduced maximum rise induced by SAR of 0.0479°C occurs.

The largest temperature increase associated with the operation of the retinal prosthesis has been shown to be due to the power dissipated by the stimulator IC, which has been evaluated under different operational conditions, corresponding to various degrees of damage of the patient's retina, and different choroidal blood flow assumptions. A worse case temperature rise of 0.6123°C in the eye with the implant in the absence of blood flow and a reduced peak increase of 0.4349°C when accounting for blood flow has been recorded when computing the temperature increase associated with the implanted microchip. It should be noted, however, that maximum temperature increase induced on the retina, the most delicate organ in the human eye, was lower than 0.2°C when the implanted microchip was collocated in the center of the eyeball.

We should note that the computed results closely parallel recent experimental results in animals, especially for the case of absence of choroidal blood flow. This suggests that actual choroidal blood flow rates are not such to enforce a constant 37°C on the choroid, as in the case of "infinite" blood flow. Three-dimensional modeling will be considered to provide additional data in support of these observations.

References

[1] S.C. DeMarco, S.M. Clements, and W. Liu. "A 60 Channel Implantable Neuro-stimulator for an Epi-Retinal Visual Prosthesis". (Unpublished).

[2] P.R. Troyk and M.A.K. Schwan. "Closed-loop class E transcutaneous power and data link for MicroImplants". *IEEE Transactions on Biomedical Engineering*, 39(6):589–599, June 1992.

[3] W.K. Noell, V.S. Walker, B.S. Kang, and et al. "Retinal damage by light in rats". *Investigative Ophthalmology and Visual Science*, 5:450, 1966.

[4] E. Friedman and T. Kuwubara. "The retinal pigment epithelium: IV. The damaging effects of radiant energy". *Archives of Ophthalmology*, 80:265–279, 1968.

[5] L.M. Parver, C. Auker, and D.O. Carpenter. "Choroidal blood flow as a heat dissipating mechanism in the macula". *AM J Ophthalmol*, 89:641–646, 1980.

[6] J.T. Ernest. "Choroidal circulation". In Stephen J. Ryan, editor, *Retina*, volume 1: Basic Science and Inherited Retina Disease, pages 76–80. Mosby-Year book, Inc., 2 edition, 1994.

[7] Peter W.V. Gurney. "Is our 'inverted' retina really a 'bad design'?". *Creation Ex Nihilo*, 13(1), 1999. also online at http://www.trueorigins.org/retina.htm as January 2000.

[8] L.M. Parver, C. Auker, and D.O. Carpenter. "Choroidal blood flow: III. Reflexive control in the human". *Archives of Ophthalmology*, 101:1604, 1983.

[9] L.M. Parver. "Temperature modulating action of choroidal blood flow". *Eye*, 5:181, 1991.

[10] F. Bardati, G. Gerosa, and P. Lampariello. "Temperature distribution in simulated living tissues irradiated electromagnetically". *Alta Frequenza*, XLIX(2):61–67, 1980.

[11] D.V. Piyathaisere, E. Margalit, S.J. Chen, J.S. Shyu, S.A. D'Anna, J.D. Weiland, R.R. Grebe, L. Grebe, G. Fujii, S.Y. Kim, R.J. Greenberg, Jr. E. De Juan, and M.S. Humayun. "Heat Effects on the Retina". Submitted July 3rd, 2001 to *Ophthalmic Surgery and Lasers*.

[12] M.S. Humayun, E. De Juan, Jr., G. Dagnelie, R.J. Greenberg, R.H. Propst, and H. Phillips. "Visual perception elicited by electrical stimulation of the retina in blind humans". *Archives of Ophthalmology*, 114:40–46, 1996.

[13] M.S. Humayun, E. De Juan, Jr., J.D. Weiland, G. Dagnelie, S. Katona, R. Greenberg, and S. Suzuki. "Pattern electrical stimulation of the human retina". *Vision Research*, 39:2569–2576, 1999.